DOI: 10.1002/chem.201100173

Thermodynamics, Structure and Properties of Polynuclear Lanthanide Complexes with a Tripodal Ligand: Insight into their Self-Assembly

Josef Hamacek,*[a] Céline Besnard,[b] Tiphaine Penhouet,[c] and Pierre-Yves Morgantini[c]

Abstract: Self-assembly processes between a tripodal ligand and Ln^{III} cations have been investigated by means of supramolecular analytical methods. At an equimolar ratio of components, tetranuclear tetrahedral complexes are readily formed in acetonitrile. The structural analysis of the crystallographic data shows a helical wrapping of binding strands around metallic cations. The properties of this series of highly charged 3D compounds were examined by using NMR spectroscopy and optical methods in solution and in the solid state. In the presence of excess metal, a new trinuclear complex was identified. The X-ray crystal structure elucidated the coordination of metallic cations with two ligands of different conformations. By varying the metal/ligand ratio, a global speciation of this supramolecular system has been evidenced with different spectroscopic methods. In addition, these rather complicated equilibria were successfully characterised with the thermodynamic stability constants. A rational analysis of the self-assembly processes was attempted by using the thermodynamic free energy model and the impact of the ligand structure on the effective concentration is discussed.

Keywords: helical structures · lanthanides · polynuclear complexes · thermodynamics · tripodal ligands

Introduction

The particular optical and magnetic properties of Ln^{III} ions have motivated coordination chemists to prepare discrete supramolecular assemblies to get new functional materials.[1] In this context, the incorporation of Ln^{III} as functional centres in molecular edifices has found various applications, such as lighting[2] and light-conversion devices,[3] optical fibres,[4] luminescent probes[5] and switches,[6] near-IR emitting materials[7] and contrast agents in medical imaging.[8] Each of these specific applications requires a suitable organic receptor, the design of which must ensure the desired properties of an assembly, such as thermodynamic and kinetic stability, good sensitisation of Ln^{III} luminescence or the presence of exchangeable protons in the first coordination sphere. To get these pre-organised ligands, the synthetic strategies mainly take advantage of the attachment of polydentate coordination moieties on a suitable platform, such as small macrocycles[9] or polyamines.[10] Reducing these platforms to a single atom provides podand-like ligands with different degrees of denticity, which is particularly useful for a fine tuning of coordination cavities for Ln^{III}. A large family of tripodal ligands with mostly carbonylpyridine-derived segments is obtained by anchoring binding strands on a nitrogen atom, as illustrated with **L1**–**L6**.[11–16] Alternatively, a carbon atom is a convenient choice and has been applied by Piguet et al. for investigating the tripodal complexes with **L7**[17] and **L8**.[18] The reaction of tripodal ligands with Ln^{III} provides mainly mononuclear complexes, which intriguingly do not exhibit a high stability compared with macrocyclic receptors with better predisposed coordinating atoms. Nevertheless, the flexibility of tripodal ligands may enhance the interactions between donor atoms and metal ions and reduce size-discrimination effects. The intrinsic pre-organisation of ligands can be measured with the effective concentration, c^{eff}, which corresponds, by definition, to the entropic difference between inter- and intramolecular binding. The value of c^{eff} can be calculated from the stability constants of related complexes by using thermodynamic modelling. This innovative approach in supramolecular chemistry aims to identify and quantify key energetic parameters for a better understanding of self-assembly pro-

[a] Dr. J. Hamacek
Department of Inorganic, Analytical and Applied Chemistry
University of Geneva, 30 quai E.-Ansermet
1211 Geneva 4 (Switzerland)
Fax: (+41) 22-379-6830
E-mail: Josef.Hamacek@unige.ch

[b] Dr. C. Besnard
Laboratory of X-ray Crystallography
University of Geneva, 24 quai E.-Ansermet
1211 Geneva 4 (Switzerland)

[c] Dr. T. Penhouet, Dr. P.-Y. Morgantini
Department of Physical Chemistry
University of Geneva, 30 quai E.-Ansermet
1211 Geneva 4 (Switzerland)

Supporting information for this article is available on the WWW under http://dx.doi.org/10.1002/chem.201100173 and contains the results of structural, photophysical, NMR spectroscopy, ESMS and thermodynamic analyses (Tables S1–S11); NMR spectra of the Ln^{III} complexes (Figure S1); spectrophotometric titration with Lu^{III} (Figure S2); luminescence spectra (Figures S3–S5), structural characterizations of $[Lu_3\mathbf{L10}_2]^{9+}$ (Figures S6–S11); distribution curves for Lu^{III} complexes (Figure S12); statistical factors (Figure S13); computations of the effective concentration for $\mathbf{L1}^a$; and additional crystallographic data for $[Lu_3\mathbf{L10}_2]^{9+}$ (Figure S14).

cesses.[19,20] Although the tripodal ligands seem to be sufficiently pre-organised to coordinate Ln^{III} cations, recent thermodynamic studies revealed a low value for the effective concentration in tripodal complexes.[18] This finding gives quantitative evidence for unfavourable intramolecular reactions within the self-assembly and translates in a drastic decrease in thermodynamic stability. In addition to entropic factors, the introduction of structural constraints, that is, shortening of the spacer length between the anchoring atom and binding sites (**L9**,[21] **L10**[22]), and a mismatch between the ligand denticity and the Ln^{III} coordination number[14] may prevent the formation of mononuclear tripodal complexes. Consequently, self-assembly leads to polynuclear structures with opened binding strands of a tripodal ligand (a trefoil form) that coordinate to different metal ions.

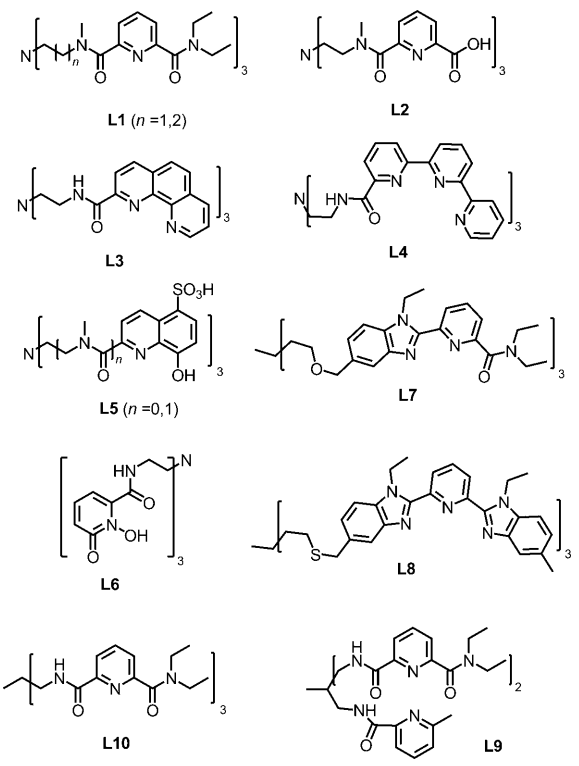

We report here on the detailed characterisation of self-assembly processes between a short tripodal ligand (**L10**) and lanthanide cations. Mixing of equivalent amounts gives tetrahedral lanthanide helicates that have been partially described in a recent communication.[22] The formation of these multicomponent assemblies is energetically favourable due to the trefoil form of the ligand. Despite few lanthanide-containing three-dimensional edifices described in the literature,[23] our system represents a rare example of polynuclear lanthanide complexes in which the self-assembly is directed and controlled by the ligand structure. These three-dimensional discrete complexes may potentially act as functional materials with interesting paramagnetic and luminescent properties. The latter will be elucidated herein with photophysical studies. A methodical combination of crystallography, ^{1}H NMR spectroscopy, ESMS and spectrophotometry allows a reliable characterisation of Ln^{III} tetrahedral complexes along the series as well as other complexes formed at different stoichiometries. More particularly, we will carry out the investigations of trinuclear complexes formed and isolated in the presence of excess metal. These unusual assemblies extend the family of few complexes with a triangular topology of Ln^{III} cations.[14,24] Finally, the stability constants of different complex species and their analysis with thermodynamic modelling will be discussed.

Results and Discussion

Preparation and characterisation of the $[Ln_4L10_4]^{12+}$ (Ln=La–Lu, Y) complexes: The reaction of Ln^{III} perchlorates with **L10** at stoichiometric conditions (1:1) results in tetrahedral $[Ln_4L10_4]^{12+}$ complexes.[22] The complexes with Ln=Nd, Eu, Gd, Tb, Yb, Lu and Y were isolated in the solid state and characterised by using elemental analyses, NMR spectroscopy and ESMS (see Tables S1–S3 and Figure S1 in the Supporting Information). We predict that isostructural complexes with other lanthanides may be prepared using analogous procedures by taking into account their similar cationic size. The only exception was observed for La^{III} complexes, in which the NMR spectrum of the isolated compound shows large unresolved bands (Figure S1c), which may be attributed to a mixture of low-symmetry species undergoing chemical exchange processes. The isolated compounds are soluble in acetonitrile, but the presence of a stronger coordinating solvent leads to the dissociation of coordination bonds with **L10**. This behaviour was examined by adding water to a solution of $[Eu_4L10_4][ClO_4]_{12}$ in acetonitrile. The tetranuclear complex starts to hydrolyse at a $\approx$30-fold excess of water per metal ion and its complete destruction is achieved at 2.5% (v/v) of water. In these conditions, the unresolved and broad NMR spectrum indicates the presence of various exchanging complexes. Further water addition eventually provokes the release of free **L10**. A partial dissociation of the tetranuclear complex has also been observed in methanol.

Crystal structure of the $[Tb_4L10_4]^{12+}$ cation: To demonstrate the helical character of tetrahedral complexes, the crystal structure of $[Tb_4L10_4]^{12+}$ (Figure 1) was analysed in detail. The ligand strands are coordinated to three different terbium cations and impose an identical helicity around all cations in the complex. Therefore, the resulting complexes correspond to the mixture of enantiomers.

According to the early definition,[25] helicates were characterised as strands wrapped around a helical axis defined by at least two metallic cations. In our case, the helical axis is identical with a threefold axis going through the metallic cation and C1 of the ligand, which is not coordinated to this cation. This arrangement is similar to non-covalently pre-or-

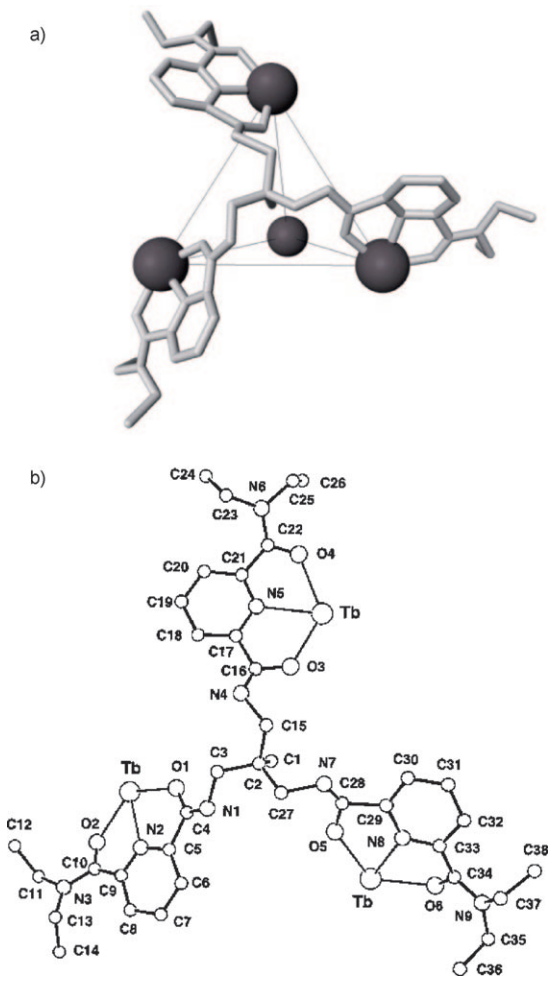

Figure 1. a) Detailed view of the coordination environment around Tb^{III} cations in $[Tb_4\mathbf{L10}_4]^{12+}$. b) Atom numbering scheme in the crystal structure.

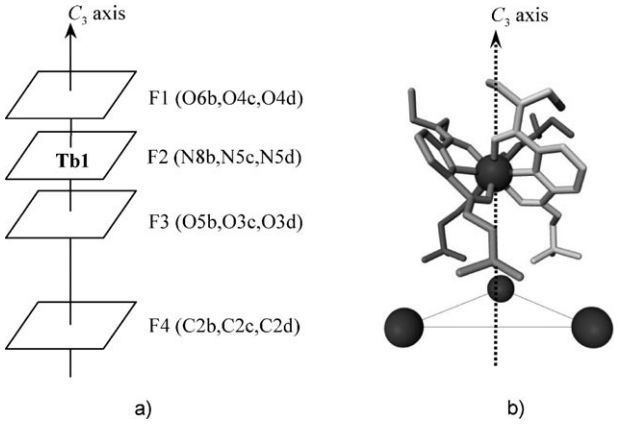

Figure 2. Coordination sphere around metallic cations in $[Tb_4\mathbf{L10}_4]^{12+}$. a) Schematic representation of four facial planes with the donor atoms. b) Wrapping of three different binding strands around one terbium cation (hydrogen atoms are omitted for clarity).

ganised tripods,[26] except that the capping part is comprised of a three-metal platform, that is, three cations coordinated to the same ligand. The organisation of the ligand strands around metallic cations is close to that in the complexes formed with the simple ligand 2,6-bis(*N*,*N*-diethylcarbamoyl)pyridine (**L11**).[27] Three strands of three different **L10** ligands (Figure 2) are wrapped around the terbium cation with an average pitch for all Tb cations of 10.8(7) Å (for helical portions between planes F1–F2 and F2–F3, Table S4), which compares well with 11.84/13.3 Å for **L1**, 11.55 Å found for **L2** and 11.32 Å for **L11**. The helical pitch for the more flexible part between planes F3 (O5b, O3c, O3d) and F4 (C2b, C2c, C2d) is about 130(20) Å, which is a quite modest value (Table S4). The coordination environment of each Tb^{III} can be described as a distorted tricapped trigonal prismatic site. The Tb^{III} cations almost lie in the F2 plane defined by the threefold-symmetry-related pyridine nitrogens. The distance between the trigonal faces of the prism defined by carbonyl oxygens (F1, F3) and F2 is 1.60(3) Å, which differs from the irregular distances found within tripodal $[Eu\mathbf{L1}]^{3+}$ complexes. Consequently, the helicity around the terbium cations is regular within the edifice. The average Tb–O amide bond length (Table S5) falls in the range of values previously reported for Eu^{III} complexes with **L1** and **L11**. Nevertheless, the Tb–O bonds closer to the centre of the tetrahedron (2.42(3) Å) are a little longer than those of the more distant ones (2.38(2) Å). The Tb–N bond length (2.53(2) Å) is slightly shorter than in $[Eu\mathbf{L1}]^{3+}$ complexes (2.55–2.57 Å).

A closer inspection of the crystal structure of $[Tb_4\mathbf{L10}_4]^{12+}$ also shows that the space inside the complex is not sufficient to accommodate any molecule and the complex may be considered as a void cage. In the crystal structure, all CH_3 groups attached to the ligand anchor are pointing to the tetrahedron centre (C^T) with the average distance $d(C1–C^T) = 2.77(6)$ Å. These protons are thus placed in the cage and we denote this particular conformation of **L10** as *endo*-CH_3.

Electronic and photophysical properties of L10 and $[Ln_4\mathbf{L10}_4]^{12+}$ complexes: In acetonitrile, ligand **L10** shows a broad and asymmetric band envelope centred around $\lambda = 270$ nm and assigned to a combination of $n\rightarrow\pi$ and $\pi\rightarrow\pi^*$ transitions centred onto the pyridinecarboxamide units as previously reported for **L1**,[11] **L2**[12] and **L11**.[27] Similarly, the absorption spectrum is significantly modified upon complexation to Ln^{III} and a broad absorption becomes structured with 1) a bathochromic shift of the peak maximum ($\lambda = 279$ nm), 2) an increase in intensity and 3) the appearance of shoulders on both high- and low-energy sides (Figure S2). A parallel behaviour is observed for **L10** in the solid state. Excitation via the ligand-centred excited states produces a weak broad fluorescence band originating from $^1\pi\pi^*$ levels (Figure 3a). Time-resolved spectra of **L10** (10–200 μs) show a residual short-lived emission at the same energy that originates from the $^3\pi\pi^*$ levels with a lifetime, τ, of <50 μs (Figure S3a). The residual emission is centred about $\lambda = 476$ nm. Similar behaviour was observed for the $[Gd_4\mathbf{L10}_4]^{12+}$ complex (Figures S3b and S4, Table S6). This points to the exis-

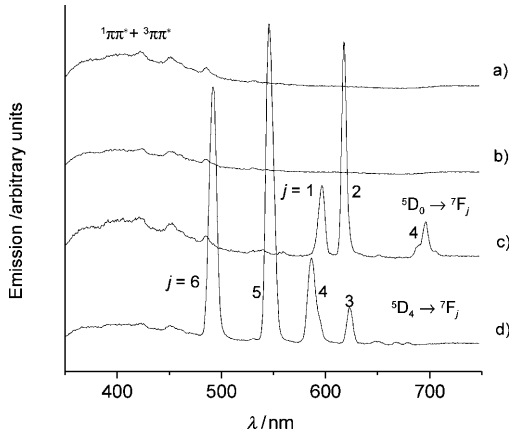

Figure 3. Fluorescence spectra of a) **L10**, b) $[Gd_4\mathbf{L10}_4][ClO_4]_{12}$, c) $[Eu_4\mathbf{L10}_4][ClO_4]_{12}$ and d) $[Tb_4\mathbf{L10}_4][ClO_4]_{12}$ in the solid state at 77 K ($\lambda_{ex}=279$ nm).

tence of efficient nonradiative deactivation pathways, as previously reported for **L1**[11] and **L11**.[27]

Luminescent properties of $[Eu_4\mathbf{L10}_4]^{12+}$ in the solid state: The emission spectra of $[Eu_4\mathbf{L10}_4][ClO_4]_{12}$ were obtained upon irradiation of the ligand-centred excited states (35 840 cm^{-1}). The low-resolution emission spectra at room temperature show relatively intense $^5D_0 \rightarrow {}^7F_j$ ($j=1$, 2, 4) transitions, which become structured at lower temperatures (Figures 3 and S4). The observation of the metal-centred transitions together with a broad residual emission of the ligand-centred excited states confirms a poor antenna effect combined with an inefficient **L10**$\rightarrow$Ln^{III} energy transfer. To get a better insight into the geometry of the complex, we performed a high-resolution measurement of luminescence at 10 K with Eu^{III} as a structural probe (Figure 4, Table S7). The symmetry-sensitive transitions Eu($^5D_0 \rightarrow {}^7F_0$) show a unique band, which indicates the presence of one crystallographic site that is compatible with the T symmetry of $[Tb_4\mathbf{L10}_4][ClO_4]_{12}$ in the crystal structure. Moreover, the very weak intensity of this transition is compatible with the local C_3 symmetry, for which this transition is forbidden by the Laporte rule. Two main components are observed for Eu($^5D_0 \rightarrow {}^7F_1$) transition, for which the latter is slightly split into two components.[11,27] The $^5D_0 \rightarrow {}^7F_2$ transition displays a band with a maximum at $\lambda=617$ nm composed of five components. The Eu($^5D_0 \rightarrow {}^7F_4$) transition displays a series of six bands with a maximum at $\lambda=694$ nm. The overall splitting profile is thus compatible with the local C_3 site symmetry despite minor deviations from the ideal case.

The Eu($^5D_0$) lifetime (1.79 ms at 77 K, solid state) is slightly longer than that of $[Eu\mathbf{L1}][ClO_4]_3$ (1.45 ms) and comparable to that of protonated complex $[Eu(\mathbf{L1}+H^+)][CF_3SO_3]_4$ (1.81–1.87 ms)[11] and $[Eu\mathbf{L11}_3][CF_3SO_3]_3$ ($\tau=$ 1.93 ms).[27] These observations points to a negligible contribution from the amide linker oscillators (N–H) to the deactivation pathway of the Eu($^5D_0$) level and suggest efficient protection of the metallic site from external interactions due to the helical arrangement of binding strands. The luminescent lifetimes do not exhibit a significant dependence on temperature (Table 1).

Table 1. Observed lifetimes of Eu^{III} and Tb^{III} at various temperatures in the solid state and in solution in degassed acetonitrile.

	λ_{ex} [cm^{-1}]	τ [ms]		
		77 K	295 K	295 K (CH_3CN)
$[Eu(\mathbf{L11})_3][CF_3SO_3]_3$[27]	32468	1.93(3)	–	
$[Eu\mathbf{L1}][ClO_4]_3$[11]	28170	1.45(3)	1.09(2)	–
$[Eu(\mathbf{L1}+H^+)][CF_3SO_3]_3$[11]	32470	1.87(6)	1.81(1)	–
$[Eu(\mathbf{L1}+H^+)][CF_3SO_3]_3$[11]	25320	1.80(1)	1.50(1)	1.96(3)
$[Eu_4\mathbf{L10}_4][ClO_4]_{12}$	35842	1.79(1)	1.76(1)	1.85(3)
$[Tb_4\mathbf{L10}_4][ClO_4]_{12}$	35842	1.61(1)	1.45(1) ($^7F_5$)	1.51(1)
$[Tb_4\mathbf{L10}_4][ClO_4]_{12}$	30490		1.32(1) ($^7F_5$)	

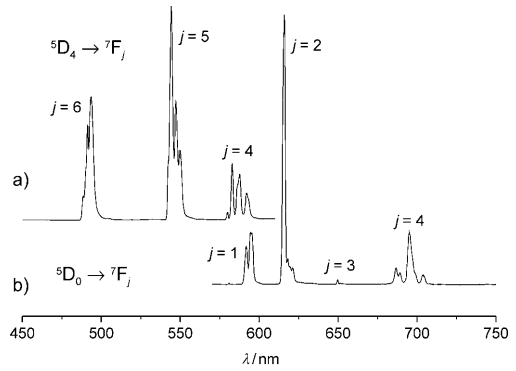

Figure 4. High-resolution luminescence spectra of a) $[Tb_4\mathbf{L10}_4][ClO_4]_{12}$ and b) $[Eu_4\mathbf{L10}_4][ClO_4]_{12}$ at 10 K ($\lambda_{ex}=279$ nm).

The energy corresponding to $^5D_0 \leftarrow {}^7F_0$ transitions is influenced by the composition of the Eu^{III} coordination sphere, which modifies the total charge on Eu^{III} through the nephelauxetic effect. This energy at 295 K can be predicted with the equation described by Frey and Horrocks [Eq. (1)],[28] in which $\tilde{\nu}_0$ is 17 374.0 cm^{-1} for the free metal ion, C_{CN} accounts for one for the nine-coordinated Eu^{III} cation, n_i is the number of atoms of type i, and δ_i is the capacity of the atom i to accept the electronic density of the metal ion. According to the crystal structure, the coordination sphere of each Eu^{III} ion is nine-coordinated by six oxygen atoms of carboxamide groups ($\delta_i=-15.7$ cm^{-1}) and three heterocyclic nitrogen atoms ($\delta_i=-15.3$ cm^{-1}).[11,27]

$$\tilde{\nu} = \tilde{\nu}_0 + C_{CN}\sum n_i\delta_i \quad (1)$$

The application of Equation (1) gives the energy of 17 234 cm^{-1} at 295 K. The excitation spectrum of $[Eu_4\mathbf{L10}_4]$-

$[ClO_4]_{12}$ at 10 K reveals the symmetrical band of a $^5D_0 \leftarrow {}^7F_0$ transition centred at $\tilde{\nu}_{exp} = 17232\ cm^{-1}$ ($\lambda = 580.322$ nm). This corresponds to 17244 cm^{-1} at 295 K after taking into account the temperature correction of 1 cm^{-1} per 24 K. This experimental value is very close to that measured for $[Eu\mathbf{L1}]^{3+}$ (17225 cm^{-1})[11] and $[Eu\mathbf{L11}_3]^{3+}$ (17227 cm^{-1})[27] and in qualitatively good agreement with the calculated value.

In acetonitrile, the emission spectra of $[Eu_4\mathbf{L10}_4]^{12+}$ (Figure S5) closely match the data obtained in the solid phase. Nevertheless, the Eu($^5D_0$) lifetime is slightly longer (1.85(3) ms), as also observed for complexes with **L1**. It confirms that no water molecules are present in the first coordination sphere. The quantum yield of $[Eu_4\mathbf{L10}_4]^{12+}$ relative to $[Eu(terpy)_3]^{3+}$[29] (terpy = terpyridine) is weak and amounts to $\Phi_{rel} = 4.6 \times 10^{-2}$ ($\Phi_{abs} = 6.0 \times 10^{-4}$). However, this value is much higher than the quantum yields determined for $[Eu\mathbf{L11}_3]^{3+}$ ($\Phi_{rel} = 6.6 \times 10^{-3}$)[27] or for the protonated tripodal complex $[Eu(\mathbf{L1}{+}H)]^{3+}$ ($\Phi_{rel} = 1.1 \times 10^{-2}$).[11] Because the composition of the Eu^{III} coordination sphere remains unchanged, the enhancement of the metal-centred emission may result from a higher probability of the intramolecular energy transfer within tetranuclear assemblies.

To get information on the coordination sphere of Eu^{III} on dissolving the complex in methanol, we have resorted to empirical Equation (2) that relates the quenching efficiencies of CH_3OH and CD_3OD.[30] The luminescent lifetimes were determined for $[Eu_4\mathbf{L10}_4]^{12+}$ dissolved in normal and deuterated methanol ($\approx 1 \times 10^{-5}$ M) and amount to $\tau_H = 0.72$ ms and $\tau_D = 1.94$ ms, respectively.

$$n = 2.1\left(\frac{1}{\tau_H} - \frac{1}{\tau_D} - 0.125\right) \qquad (2)$$

By applying Equation (2), we estimate the number of coordination sites occupied by CH_3OH as equal to $n = 1.6 \pm 0.5$. This value corresponds to approximately 1 to 2 molecules of bound CH_3OH per metal ion and clearly indicates a partial decomplexation of lanthanides in this polar solvent. This observation is also confirmed with the NMR spectrum of $[Eu_4\mathbf{L10}_4][ClO_4]_{12}$ in CD_3OD. Indeed, the fingerprint peak at ≈13 ppm (H1) disappears and the spectrum is badly resolved. This indicates complete destruction of the tetranuclear complexes.

Luminescent properties of $[Tb_4\mathbf{L10}_4][ClO_4]_{12}$: The low-resolution emission spectra of $[Tb_4\mathbf{L10}_4][ClO_4]_{12}$ in the solid state were obtained upon irradiation through ligand-centred excited states ($\lambda = 279$ nm, Figure 3d). Single bands were observed for $^5D_4 \rightarrow {}^7F_j$ ($j = 0,1$) transition at 77 K ($\lambda = 679$, 667.5 nm), whereas a large band for $^5D_4 \rightarrow {}^7F_2$ was observed at $\lambda = 647.5$ nm. The $^5D_4 \rightarrow {}^7F_4$ transition is split into three components. The intense transitions $^5D_4 \rightarrow {}^7F_j$ ($j = 5,6$) are observed at $\lambda = 545$ and 493 nm, respectively. The high-resolution emission spectrum was recorded at 10 K and shows the structured emission bands for the $^5D_4 \rightarrow {}^7F_j$ transitions (Figure 4). The Tb($^5D_4$) lifetime (1.61 at 77 K, Table 1) is comparable to that of $[Tb\mathbf{L1}]^{3+}$ and also points to a negligible deactivation through the amide N–H oscillators. The emission spectrum of $[Tb_4\mathbf{L10}_4]^{12+}$ in acetonitrile is reminiscent of that in the solid state, with a relatively low emission from the ligand-centred excited states (Figure S5).

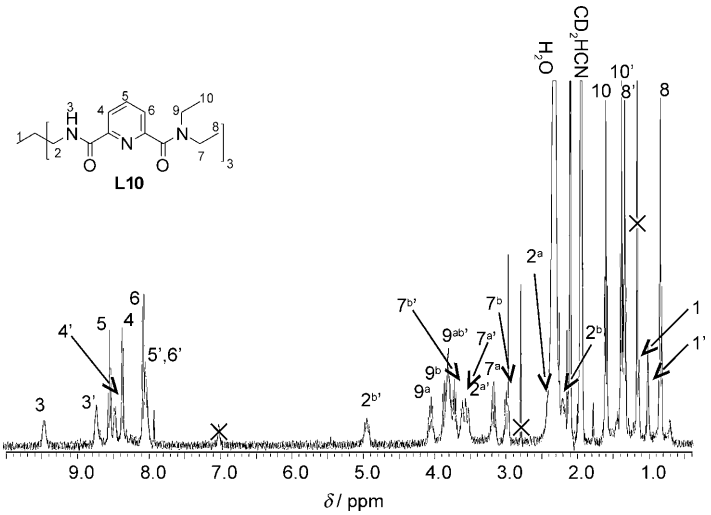

Figure 5. ^{1}H NMR spectrum of $[Lu_3\mathbf{L10}_2][ClO_4]_9$ with the peak assignments (CD_3CN, 298 K).

Preparation and characterisation of the $[Ln_3\mathbf{L10}_2]^{9+}$ complexes (Ln = Eu, Lu): The trinuclear complexes were prepared by directly mixing Ln^{III} perchlorates with **L10** in a molar ratio of 3:2 or by adding the metal salt to a solution of $[Ln_4\mathbf{L10}_4]^{12+}$ in acetonitrile. These complexes were isolated in the solid state by diffusion of *tert*-butylmethylether into the acetonitrile solution followed by filtration of the white precipitate. The elemental analysis of isolated microcrystals gives the composition $[Ln_3\mathbf{L10}_2][ClO_4]_9 \cdot 6H_2O$ (Table S1). The ESMS spectra of isolated compounds show the presence of the $[Ln_3\mathbf{L10}_2]^{9+}$ species and the $[Ln\mathbf{L10}]^{3+}$ species, which results from an easy decomposition of the complex under the given experimental conditions (Figure S6). The NMR spectra of the lanthanide complexes (Ln = Eu, Lu) consist of two sets of peaks of equal intensities, which were attributed by using COSY and T_1 NMR techniques (Table S8). This pattern is compatible with two differently coordinated C_3-symmetrical ligands, the proton signals of which exhibit different chemical shifts compared with the signals of **L10** and $[Ln_4\mathbf{L10}_4]^{12+}$ (Figure 5). The striking difference in the coordination mode of ligands is also evidenced with the chemical shift of protons belonging to the anchoring methyl group, which serves as a structural probe in $[Eu_3\mathbf{L10}_2]^{9+}$. Indeed, one methyl singlet is observed at $\delta = 3.5$ ppm and the second at $\delta = -6.8$ ppm. The observation of diastereotopic methylene protons is typical for a helical arrangement and indicates the wrapping of ligand strands about metallic cations. However, the large splitting observed for the H2 protons, even in the diamagnetic complex $[Lu_3\mathbf{L10}_2]^{9+}$ ($\Delta\delta = 1.4$ ppm), is remarkable (Table S8).

The variable temperature experiments (294–343 K) showed only minor chemical shift differences detectable mostly for aromatic protons. This means that the structures of trinuclear species do not undergo significant changes in solution over the examined temperature range (Figure S7).

Crystal structure of the cation $[Lu_3L10_2]^{9+}$: X-ray quality crystals were obtained for the Lu^{III} complex by diffusion of *tert*-butylmethylether into a concentrated solution of $[Ln_3\mathbf{L10}_2]^{9+}$ in acetonitrile (Figure 6, Figure S8). A summary

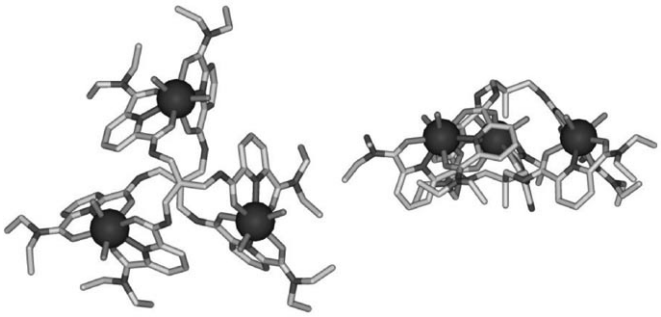

Figure 6. Crystal structure of $[Lu_3\mathbf{L10}_2]^{9+}$: a) top view along the threefold axis; b) side view.

of related crystal data is given in reference [31] and more details on the structure refinement can be found in the Supporting Information. The crystallographic analysis indeed shows the formation of a trinuclear complex in which the Lu^{III} cations are coordinated with two ligands within the vertices of a regular triangle with a d(Lu–Lu) value of 8.776(8) Å, which is about 1 Å shorter than in $[Tb_4\mathbf{L10}_4]^{12+}$ (9.83 Å). Each cation is octacoordinated by two tridentate sites of two **L10** and the coordination sphere is completed by two water molecules. The coordination polyhedron around Lu^{III} can be described as a strongly distorted antiprism (Figure S9). The lengths of coordination bonds are about 0.1 Å shorter than in $[Tb_4\mathbf{L10}_4]^{12+}$, most probably due to stronger electrostatic interactions in Lu^{III} complexes, and are listed in Table S9. Confirming previous NMR spectroscopic analyses, the complex is indeed C_3 symmetrical with the threefold axis going through anchoring carbon atoms of both ligands (C23 and C44, Figure S8). The structure of $[Ln_3\mathbf{L10}_2]^{9+}$ is topologically comparable with the trinuclear sandwich-like complex formed with terpy-based tripodal ligand **L4**,[14] but the latter exhibits a D_3 symmetry. Here, the coordinated ligands are conformational isomers that adapt for the best coordination to lanthanide cations by rotation around CH_2–NH bonds. The first ligand is folded around the methyl protons of the anchor and adopts an *endo*-CH_3 conformation. The second ligand is almost spread in plane with an *exo*-CH_3 orientation of methyl protons (Figure S10). Two water molecules coordinated to each metal ion are not hindered and would be easily exchangeable in solution. Interestingly, the Flack parameter is found to be $x=0.061(12)$ and this chiral crystal structure thus contains 94(1)% of the complex with the helicity *M*. However, dissolving solid $[Lu_3\mathbf{L10}_2]^{9+}$ in acetonitrile gives a racemic mixture with no optical activity.

Dynamic properties of the $[Ln_4L10_4]^{12+}$ and $[Ln_3L10_2]^{9+}$ complexes in solution: Information about the size and the molecular weight of compounds in solution may be conveniently achieved with DOSY-NMR (diffusion-ordered spectroscopy) that provides access to the translational self-diffusion coefficients, D.[32] The value of D for the tetranuclear Eu^{III} complex was reported in a previous communication[22] and used for estimating its molecular weight M_w in solution according to the Einstein–Smoluchowski–Stokes auto-diffusion theory [Eq. (3)], in which $\bar{\nu}$ is the specific molecular volume, which gives a value that is about 56% more than the expected value.

$$\frac{D_x}{D_r} = \sqrt[3]{\frac{\bar{\nu}_r (M_r)_r}{\bar{\nu}_x (M_r)_x}} \tag{3}$$

Taking into account this significant difference between theoretical and experimental values, we have decided to shed more light on these discrepancies by evaluating the hydrodynamic radius (r_H; radius of the moving cation) of these highly charged particles.[33] For this purpose, the Stokes–Einstein equation [Eq. (4)] may be used for molecules generally bigger than $r_H=15$ Å with $c=6$ (η is the fluid viscosity).

$$D_x = \frac{kT}{c\pi\eta r_H^x} \tag{4}$$

However, for medium-sized molecules, factor c must be expressed as a function of r^{solv}/r_H^x according to the microfrictional theory,[34] in which r^{solv} is the solvent hydrodynamic radius (i.e., acetonitrile). Finally, the additional semi-empirical improvement introduced by Chen[35] leads to Equation (5).

$$D_x = \left(\frac{kT}{6\pi\eta r_H^x}\right)\left(1 + 0.695\left(\frac{r^{solv}}{r_H^x}\right)^{2.234}\right) \tag{5}$$

For non-spherical molecules, another shape-related correction factor ($f(p)$; p is a geometrical factor) must be considered; it relates r_H^x to the radius r_{eq}^x expected for a sphere of the equivalent volume like so: $r_H^x = r_{eq}^x/f(p)$.[36] However, the shape of the tetranuclear complex and of $[Ru(bipy)_3]^{2+}$ (used as the reference; bipy = bipyridine), is reasonably approximated as a sphere (an average distance from the centre of the tetrahedron to each Tb in $[Tb_4\mathbf{L10}_4]^{12+}$ is 6.0 Å) and thus we expect that $f(p)\cong 1$ for both. The radius r_{eq}^x of the complex can be estimated from the volume limited by the Conolly surface accessible to solvent molecules (probe radius $r_{eq}^{solv}=2.0$ Å for acetonitrile).[32] The latter is constructed around the molecular structure in the crystalline state as a model (i.e., the Connolly volume).[37] The volume deter-

mined for the crystal structure of $[Tb_4\mathbf{L10}_4]^{12+}$ amounts to 3305 Å^3 and we easily access a radius of $r^x_{eq}=9.24$ Å. If we expect that $r^x_{eq}\cong r^x_H$ for spherical molecules, the correction factor in Equation (5) may be approximated with $r^{solv}/r^x_H = r^{solv}_{eq}/r^x_{eq}$. These considerations allowed us to calculate the corresponding value of r^x_H by using previously measured diffusion coefficients (Table S10).[22] Consequently, the hydrodynamic radius of $[Ru(bipy)_3]^{2+}$ is equal to 4.73(7) Å, which compares well with the literature value ($r_H^{[Ru(bipy)_3]}=$ 4.75 Å).[20] In the case of the tetrametallic complex $[Eu_4\mathbf{L10}_4]^{12+}$, the experimental hydrodynamic radius $r_H^{[Eu_4\mathbf{L10}_4]}$ is equal to 9.3(1) Å, which is in good agreement with $r_H^{[Eu_4\mathbf{L10}_4]}$ calculated above and confirms the expected pseudo-spherical shape with $r^x_{eq}/r^x_H=1$. However, this hydrodynamic radius is about 1.3 Å larger than the radius calculated from the crystallographic data ($r_{X\text{-ray}}^{[Tb_4\mathbf{L4}_4]}=8.1$ Å). This means that the specific molecular volume $\bar{\nu}_x$ in solution is significantly larger than in the solid state and than $\bar{\nu}_r$ of the reference compound $[Ru(bipy)_3]^{2+}$. The discrepancy in specific volumes thus significantly affects the determination of M_r according to Equation (3).

A similar structural analysis was undertaken for the trinuclear complex $[Ln_3\mathbf{L10}_2]^{9+}$. From the Conolly volume we calculate $r^x_{eq}=7.34$ Å by considering the spherical shape of $[Ln_3\mathbf{L10}_2]^{9+}$. DOSY-NMR spectroscopy was applied for the determination of diffusion coefficients of trinuclear complexes $[Eu_3\mathbf{L10}_2]^{9+}$ and $[Lu_3\mathbf{L10}_2]^{9+}$ and gives an average value of 6.8×10^{-10} m^{2}s^{-1} for D_x (Table S10). Interestingly, this value is only somewhat higher than the value measured for the tetranuclear complexes. However, the corresponding hydrodynamic radius ($r_H^{[Ln_3\mathbf{L10}_2]}=8.9(3)$ Å) is about 1.5 Å bigger than r^x_{eq}, and the ratio $f(p)=r^x_{eq}/r^x_H=0.83$ indicates a strong deviation from the spherical shape. Therefore, we propose to treat the shape of the trinuclear complex as an approximately disc-like ellipsoid (oblate) with $p=a/b$, in which a is the axial semi-axis and b is the equatorial semi-axis. Factor p can be easily fitted from Equation (6)[38] and the ratio $p^{-1}=b/a$ is found to be about 4.7.

$$f(p) = p^{1/3}\arctan[(1-p^2)^{1/2}/p](1-p^2)^{-1/2} \quad (6)$$

If we take the maximum value of d(C44···C24)$=7.2$ from the crystal structure (Figure S8) as a reasonable assumption for $2a$, we can estimate the equatorial axis length as about 34 Å. Although it hardly compares with the maximal diameter of $\approx$22 Å expected from the crystal structure of $[Ln_3\mathbf{L10}_2]^{9+}$, the oblate ellipsoid model seems to be more appropriate than the sphere model. The observed difference may simply reflect an insufficient agreement of the model with the crystal structure and the complex may effectively diffuse as a thinner ellipsoid. For example, if the a axis is reduced by 1.5 Å (one C–C bond, i.e., C23–C24), the equatorial axis length decreases to $\approx$27 Å, which compares better with the reality. In addition to the solvent-inaccessible volume discussed for $[Eu_4\mathbf{L10}_4]^{12+}$, the specific molecular volume of diffusing trinuclear complexes also depends on their particular shape.

Self-assembly process and thermodynamic characterisation of Ln_mL10_n complexes in solution: The speciation in the Ln^{III}–**L10** system was followed by ^{1}H NMR spectroscopy and ESMS titrations of **L10** with Eu^{III} and Lu^{III} in acetonitrile. Significant variations in the spectra were observed as the ratio $x=[Ln]_{tot}/[\mathbf{L11}]_{tot}$ was increased (Figure S11). For $x<1$ (excess of ligand), the formation of two major species (the peak maxima around $x=0.3$ and $x=0.7$) can be qualitatively distinguished in rather complicated NMR spectra. ESMS analyses show the presence of different species $[Ln\mathbf{L10}_3]^{3+}$, $[Ln_2\mathbf{L10}_3]^{6+}$ and $[Ln_3\mathbf{L10}_4]^{9+}$ during the titration, but a definitive determination of the stoichiometry of major species is difficult due to the possible fragmentation of the complexes. However, the spectra are significantly simplified for the ratio close to $x=1.0$. That is compatible with the formation of tetrahedral complexes $[Ln_4\mathbf{L10}_4]^{12+}$. Especially for $[Eu_4\mathbf{L10}_4]^{12+}$, the signal of the methyl protons H1 is strongly shifted to $\delta\approx13$ ppm due to their specific location close to the threefold axis and represents a typical fingerprint of the tetranuclear species. The ESMS spectra are reminiscent of the spectra of isolated compounds and show a series of peaks attributed to the perchlorate adducts. In the presence of excess metal ($x>1$), the NMR spectra correspond to a mixture of the tetranuclear species and a new complex. The signals of the tetranuclear complex disappear as the excess of metal increases. At about three equivalents, only two sets of sixteen signals are observed, which correspond to the spectrum of $[Ln_3\mathbf{L10}_2]^{9+}$. In addition, the signal related to uncomplexed water is shifted downfield, which is compatible with the formation of unsaturated complexes with fast exchanging solvent molecules.

Stability constants of polynuclear Ln^{III} complexes with L10: To quantitatively characterise the formation of complexes with **L10**, spectrophotometric batch titrations (3×10^{-4} M) with selected lanthanide perchlorates ($Ln(ClO_4)_3{\cdot}xH_2O$, Ln = La, Nd, Eu, Tb, Er, Lu) were carried out in acetonitrile, in which both the ligand and the Ln^{III} complexes are soluble. The solutions with $[Ln]_{tot}/[\mathbf{L10}]_{tot}=0$–5 were measured after 48 h at 25.0±0.1 °C to ensure a sufficient equilibrating. Upon complexation of Ln^{III} with **L10**, the absorption spectra show complicated variations with several breaking points suggesting the presence of different absorbing species (Figure S2). The best model for interpreting spectrophotometric data consists of the species identified in ESMS and NMR spectra. For the series of lanthanide cations from Eu^{III} to Lu^{III}, the factor analysis confirms the formation of species associated with Equilibria (7)–(10).

$$Ln^{3+} + 3\,\mathbf{L10} \rightleftharpoons [Ln\mathbf{L10}_3]^{3+} \quad \log\beta_{1,3}^{Ln,\mathbf{L10}} \quad (7)$$

$$3\,Ln^{3+} + 4\,\mathbf{L10} \rightleftharpoons [Ln_3\mathbf{L10}_4]^{9+} \quad \log\beta_{3,4}^{Ln,\mathbf{L10}} \quad (8)$$

$$4\,Ln^{3+} + 4\,\mathbf{L10} \rightleftharpoons [Ln_4\mathbf{L10}_4]^{12+} \quad \log\beta_{4,4}^{Ln,\mathbf{L10}} \quad (9)$$

$$3\,Ln^{3+} + 2\,\mathbf{L10} \rightleftharpoons [Ln_3\mathbf{L10}_2]^{9+} \quad \log\beta_{3,2}^{Ln,\mathbf{L10}} \quad (10)$$

Table 2. Stability constants of lanthanide complexes with **L10**.[a]

	$\log\beta_{1,3}^{Ln,L10}$	$\log\beta_{3,4}^{Ln,L10}$	$\log\beta_{4,4}^{Ln,L10}$	$\log\beta_{3,2}^{Ln,L10}$
La[b]				19.7(7)
Nd[c]	14.1(8)		36.2(9)	20.8(8)
Eu	14.0(4)	33.0(7)	39.4(8)	21.7(6)
Tb	15.1(5)	34.4(9)	39.7(9)	21.7(6)
Er	14.3(3)	33.2(6)	39.1(6)	21.8(4)
Lu	15.2(6)	33.0(6)	39.4(6)	23.3(5)

[a] Acetonitrile, 298 K. [b] $\text{Log}\beta_{1,2}^{La,L10}=10.6(6)$, $\log\beta_{3,3}^{La,L10}=24.3(8)$. [c] $\text{Log}\beta_{2,3}^{Nd,L10}=21.5(8)$.

The fit of spectrophotometric data with non-linear least-squares methods[39] results in the stability constants summarized in Table 2. The plot of $\log\beta$ versus the inverse ionic radius of nine-coordinate Ln^{III} (Figure 7) shows that the stability constants of all formed complexes do not significantly vary along the series except for $[Ln_3\mathbf{L10}_2]^{9+}$, in which a moderate increase agrees with the stronger electrostatic interactions expected for smaller cations. In case of Nd^{III}, the best fit is achieved with the $[Nd_2\mathbf{L10}_3]^{6+}$, $[Nd_4\mathbf{L10}_4]^{12+}$ and $[Nd_3\mathbf{L10}_2]^{9+}$ species. Interestingly, the thermodynamic stability of $[Nd_4\mathbf{L10}_4]^{12+}$ is significantly lower than that of heavier lanthanides. A better fit of spectrophotometric data is obtained with the dinuclear species $[Nd_2\mathbf{L10}_3]^{6+}$ instead of $[Nd_3\mathbf{L10}_4]^{9+}$. It is worth noting that the $[Ln_2\mathbf{L10}_3]^{6+}$ species are probably formed also with other metal ions (minor peaks in ESMS), but their small quantities ($<10\,\%$) and correlated absorption spectra prevent their detection with spectrophotometric titrations. In the case of La^{III}, the best fit of spectrophotometric data was obtained with the $[La\mathbf{L10}_2]^{3+}$, $[La_3\mathbf{L10}_3]^{9+}$ and $[La_3\mathbf{L10}_2]^{9+}$ species. As shown previously with NMR spectroscopy, the tetranuclear assemblies with bigger La^{III} cations are not thermodynamically stable. Instead we observe the formation of probably low-symmetry complexes $[La_3\mathbf{L10}_3]^{9+}$ likewise detected with ESMS in the equimolar mixture.

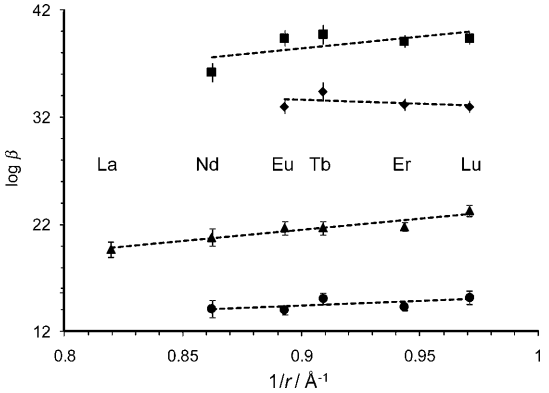

Figure 7. Variation in the stability constants for $[Ln_m\mathbf{L10}_n]$ complexes (■: $[Ln_4\mathbf{L10}_4]$, ◆: $[Ln_3\mathbf{L10}_4]$, ▲: $[Ln_3\mathbf{L10}_2]$, ●: $[Ln\mathbf{L10}_3]$) along the lanthanide series (spectrophotometry, acetonitrile, 298 K). The trendlines are guides for the eye.

According to the fitted stability constants, the distribution curves for Lu^{III} complexes, for example, are constructed in Figure S12. This demonstrates how the formation of desired supramolecular assemblies may be tuned by varying the metal/ligand ratio. The present speciation also compares well with NMR spectroscopic titrations.

Rationalisation of the self-assembly: Thermodynamic modelling has been recently developed by us for quantifying and better understanding interactions in supramolecular self-assembly processes.[19,40] The additive-free energy model is based on modelling macroscopic stability constants available for a given system with a set of appropriate microscopic thermodynamic parameters according to the general Equation (11).

$$\log\beta_{m,n}^{Ln,L}=\omega_{m,n}^{Ln,L}\omega_{m,n}^{chir}\prod_{i=1}^{inter}(f_i^{M,L})\prod_{i=1}^{intra}(c_i^{eff})\prod_{i<j}(u_{ij}^{MM})\prod_{k<l}(u_{kl}^{LL}) \tag{11}$$

The significance and origin of the microscopic descriptors in Equation (11) have been discussed in details by Piguet[41] and this thermodynamic model has already found several applications.[32,42] Herein, we will apply the modelling to the self-assembly processes occurring between Ln^{III} and **L10** [Equilibria (7)–(10)]. However, a sufficient knowledge of the structural organisation of complex species is required for evaluating the number of homo- and hetero-component interactions and the symmetry-related statistical factors. In this context, the crystal structures of $[Tb_4\mathbf{L10}_4]^{12+}$ and $[Lu_3\mathbf{L10}_2]^{9+}$ provide unambiguous information. For estimating the structure of other species, we assume the principle of maximum occupancy that predicts a predominant formation of the complexes with the highest degree of saturation for a given stoichiometry.[19] Because no reliable experimental structural information is available for $[Ln_3\mathbf{L10}_4]^{9+}$, we suggest that it may adopt a structure obtained by virtually extracting one metal ion from the tetranuclear species (Figure S13).

Taking the above assumptions into account, the correct symmetry numbers $\omega_{m,n}^{Ln,L10}$ and the chirality factors $\omega_{m,n}^{chir}$ are accessed with the explicit consideration of the solvent molecules illustrated with Equation (12). Consequently, the statistical factors $\omega_{m,n}^{Ln,L10}\omega_{mn}^{chir}$ are calculated for each species according to Equation (13) and summarised in Figure S13.

$$m\,[Ln(CH_3CN)_9]^{3+}+n\,\mathbf{L10}\rightleftharpoons[Ln_m\mathbf{L10}_n]^{12+}+36\,CH_3CN \qquad \beta_{m,n}^{Ln,L10} \tag{12}$$

$$\omega_{m,n}^{Ln,L10}\omega_{m,n}^{chir}=\frac{(\sigma_{\mathbf{L10}}\sigma_{\mathbf{L10}}^{chir})^n(\sigma_{Ln}\sigma_{Ln}^{chir})^m}{(\sigma_{Ln_m\mathbf{L10}_n}\sigma_{Ln_m\mathbf{L10}_n}^{chir})(\sigma_{CH_3CN}\sigma_{CH_3CN}^{chir})^{9m}} \tag{13}$$

The thermodynamic stability constants of the complexes $[Ln_m\mathbf{L10}_n]^{3m+}$ defined with Equilibria (7)–(10) are modelled

with Equations (14)–(17), in which $f^{Ln,\mathbf{L10}}$ is the binding affinity related to the intermolecular connection of Ln^{III} with one dicarbonylpyridine coordination site NO_2 (one coordinating nitrogen and two oxygens), u^{LL} and u^{LnLn} are interligand and intermetallic interactions, c^{eff} is the effective concentration describing an intramolecular ring-closing process. To minimize the number of fitted parameters, we assume that the intermetallic interactions and the effective concentration affecting the self-assembly are the same for all complexes despite a small difference in intermetallic distances found in $[Tb_4\mathbf{L10}_4]^{12+}$ and $[Lu_3\mathbf{L10}_2]^{9+}$ by crystallography.

$$\beta_{1,3}^{Ln,\mathbf{L10}} = 54(f^{Ln,\mathbf{L10}})^3(u^{LL})^3 \quad (14)$$

$$\beta_{3,4}^{Ln,\mathbf{L10}} = 11\,664(f^{Ln,\mathbf{L10}})^9(u^{LL})^9(u^{LnLn})^3(c^{eff})^3 \quad (15)$$

$$\beta_{4,4}^{Ln,\mathbf{L10}} = 17\,496(f^{Ln,\mathbf{L10}})^{12}(u^{LL})^{12}(u^{LnLn})^6(c^{eff})^5 \quad (16)$$

$$\beta_{3,2}^{Ln,\mathbf{L10}} = 1296(f^{Ln,\mathbf{L10}})^6(u^{LL})^3(u^{LnLn})^3(c^{eff})^2 \quad (17)$$

The multilinear fit of four parameters used for the modelling requires a minimal set of four equations and can be indeed performed for all heavier lanthanides (Eu–Lu) that produce the same speciation. A rough estimation of the microscopic parameters is summarized in Table 3, although their exact physical meaning should be considered carefully. Nevertheless, small differences in the fitted parameters along the series encourage attempts at a deeper analysis. Firstly, the binding affinity for the NO_2 site, the only energetically favourable parameter, is found to be about 25 kJ mol^{-1}, which is a somewhat lower value than the affinities fitted for linear helicates ($\approx$31 kJ mol^{-1}).[40] However, the difference is more pronounced than the value obtained by modelling of the stability constants of mononuclear complexes with **L11** [Eqns. (18)–(20); Table S11],[27] which possesses an identical NO_2 coordination site. This discrepancy is tentatively associated with the covalent connection of three binding strands in **L10** that may hinder the *trans*→*cis* conformational change of NO_2 sites upon complexation. Therefore, it is not judicious to associate the stability constants for complexes with **L11** [Eqns. (18)–(20)] to Equations (14)–(17) and to perform a simultaneous fit that indeed results in a poor correlation. The fitted energy of interligand interaction for the NO_2 site is small for all cations in comparison with the ligands containing more rigid N_3 binding sites.[18,40] Therefore, we have attempted to fix the average ΔE^{LL} value of 0.5 kJ mol^{-1} in Equations (14)–(17) and to fit the remaining three microscopic parameters from four equations. However, the fitted values differ from those in Table 3 only within statistical errors ($<$1 kJ mol^{-1}).

Table 3. Fitted microscopic thermodynamic parameters for $[Ln_m(\mathbf{L10})_n]^{3m+}$ (simultaneous least squares fits with Equations (14)–(17), acetonitrile, 298 K).[a]

Fitted parameters	Eu	Tb	Er	Lu
$\log(f_{NO_2}^{Eu,\mathbf{L10}})$/ $\Delta G_{NO_2}^{Ln,\mathbf{L10}}$ [kJ mol^{-1}]	4.12/ −23.5	4.49/ −25.6	4.32/ −24.7.6	4.65/ −26.6
$\log(f_{NO_2}^{Eu,\mathbf{L10}}c^{eff})$/ $\Delta G_{intra}^{Ln,\mathbf{L10}}$ [kJ mol^{-1}]	2.30/ −13.1	2.96/ −16.9	2.59/−14.8	0.43/ −2.4
$\log(u^{LL})/\Delta E^{LL}$ [kJ mol^{-1}]	−0.03/ 0.2	−0.03/ 0.2	−0.13/0.8	−0.17/ 0.9
$\log(u^{MM})/\Delta E^{MM}$ [kJ mol^{-1}]	−0.80/ 4.6	−1.73/ 9.9	−1.13/6.5	0.40/ −2.3
$\log(c_t^{eff})/\Delta G_{corr}^{Ln,\mathbf{L11}}$ [kJ mol^{-1}]	−1.83/ 10.4	−1.53/ 8.7	−1.73/9.9	−4.23/24

[a] Four parameters are estimated from four equations and therefore no uncertainties are given.

The intermetallic interactions in the polynuclear Ln^{III}–**L10** complexes are found to be repulsive with an average ΔE^{MM} value of 7 kJ mol^{-1} for Eu, Tb and Er, which is comparable to the energy fitted for linear helicates.[40] Conversely, the interactions are slightly attractive in the Lu complexes. Although this may be tentatively explained in terms of different solvation energies, a more reliable interpretation definitely requires an extended set of experimental thermodynamic data.

$$\beta_{1,1}^{Ln,\mathbf{L11}} = 6(f^{Ln,\mathbf{L11}}) \quad (18)$$

$$\beta_{1,2}^{Ln,\mathbf{L11}} = 12(f^{Ln,\mathbf{L11}})^2(u^{LL}) \quad (19)$$

$$\beta_{1,3}^{Ln,\mathbf{L11}} = 16(f^{Ln,\mathbf{L11}})^3(u^{LL})^3 \quad (20)$$

The energetic penalisation of intramolecular reactions amounts to about 10 kJ mol^{-1} for Eu–Er, which corresponds to a c^{eff} value of $\approx 10^{-1.7}$ M. This value is roughly comparable with the effective concentration fitted for linear helicates, in which the binding sites are separated by $\approx$9 Å ($c^{eff} \approx 10^{-1.0}$ M).[40] It reflects a relatively good preorganization of **L10** for a trefoil conformation that induces the formation of polynuclear complexes $[Ln_m\mathbf{L10}_n]^{3m+}$. However, one may alternatively expect the formation of a mononuclear tripodal complex with **L10**, by analogy with $[Ln\mathbf{L1^a}]^{3+}$.[11a,43] Why does this complex appear thermodynamically unfavourable? Let's model its stability constant with Equation (21).[18]

$$\beta_{1,1}^{Ln,\mathbf{L10}} = 12(f^{Ln,\mathbf{L10}})^3(u^{LL})^3(c_{tripod}^{eff})^2 \quad (21)$$

Note that two of the three binding events are intramolecular, which is a much higher ratio with respect to the polynuclear complexes with **L10**. Considering a relatively small ΔE^{LL}, the reaction pathway to $[Ln\mathbf{L10}]^{3+}$ is thus controlled by the magnitude of c_{tripod}^{eff}. For instance, in tripodal mononuclear complexes with **L8**, the value of c^{eff} drops by several orders of magnitude ($c_{tripod}^{eff} \approx 10^{-7.3}$ M) compared with linear helicates.[40] The effective molarity has been also estimated for tripodal complexes with $\mathbf{L1^a}$, which possesses a spacer between the NO_2 binding sites and the anchor that is longer than that of **L10** by only one CH_2. The value of $c_{tripod}^{eff} \approx 10^{-4}$ M[42] still allows the formation of tripodal complexes despite the appearance of the complexes $[Ln\mathbf{L1^a}_2]^{3+}$ in the presence of excess ligand. In the case of mononuclear complexes $[Ln\mathbf{L10}]^{3+}$, the effective concentration should be re-

duced even more ($c^{eff}_{tripod} \ll 10^{-4.0}$ M) due to significant structural strains hindering the formation of intramolecular connections. To support this hypothesis, we have optimised the molecular model of the hypothetical complex $[Eu\mathbf{L10}]^{3+}$ shown in Figure 8a. In comparison with the crystal structure of $[Eu\mathbf{L1^a}]^{3+}$ (Figure 8b), the structure of $[Eu\mathbf{L10}]^{3+}$ is elongated with apparent strains around the anchor that provoke a concomitant increase in the Eu–O lengths by 0.15 Å. This results in a drastic destabilisation of the tripodal complexes and more favourable self-assembly processes take place instead. Accordingly, the effective concentration in tripodal complexes reflects not only entropic contributions that depend on the distance between interacting binding sites[40] but also enthalpic contributions that influence the organisation of a binding cavity.

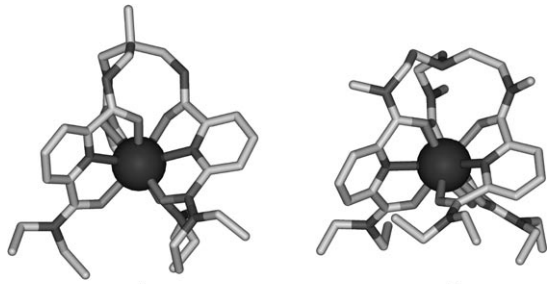

Figure 8. a) Molecular model of the tripodal europium complex with **L10**. (DFT (Perdew–Wang 91)+DZVP). b) The crystal structure of $[Eu\mathbf{L1^a}+H^+]^{4+}$.

Conclusion

The self-assembly processes occurring with trivalent lanthanides and the tripodal ligand **L10** have been investigated. At an equimolar ratio, 3D tetranuclear helicates were formed and isolated for all lanthanides along the series except La^{III}. Indeed, the thermodynamic stability of tetrahedral complexes significantly decreases for lanthanides with ionic radius $r > 1.13$ Å. Analysis of crystallographic data showed the same helicity for all binding strands, with a regular pitch on each lanthanide cation. In addition to a routine characterisation of $[Ln_4\mathbf{L10}_4]^{12+}$ with ESMS and NMR spectroscopy, the Eu^{III} and Tb^{III} complexes were used as luminescent structural probes in the solid state and in solution.

The formation of other complex species may be tuned by changing the metal/ligand ratio. ESMS, NMR spectroscopy and spectrophotometric titrations allowed us to unravel their stoichiometry and stability constants. Not surprisingly, the overall speciation also varies along the lanthanide series. Despite a considerable effort, the exact structural organisation could not be determined for the species formed at a metal/ligand ratio of <1. However, the structure of trinuclear complex $[La_3\mathbf{L10}_2]^{9+}$ assembled in the presence of excess metal was investigated by using X-ray crystallography. Surprisingly, the two coordinated ligands are not equivalent and adopt *endo*-CH_3 and *exo*-CH_3 conformations, respectively. Moreover, each metal ion in this C_3-symmetric complex is octacoordinated with two tridentate binding strands and two water molecules. The molecular size and diffusion coefficients of tri- and tetranuclear assemblies were estimated from DOSY experiments. The hydrodynamic volume measured for pseudo-spherical tetrahedral complexes is close to the Conolly volume calculated from the crystallographic data. However, this relation is not straightforward for the trinuclear species due to a strong deviation from a spherical shape. Therefore, the specific molecular volume of the supramolecular complexes appears larger when compared with the reference compound and must be explicitly taken into account for estimating molecular weights.

The thermodynamic free energy model was applied to the stability constants of lanthanide complexes formed with **L10** to estimate the microscopic parameters that control the assembly. The fitted data do not considerably vary for the complexes with heavier lanthanides. The calculated value of c^{eff} is significantly higher than expected for the formation of mononuclear tripodal complexes and explains the preferential formation of polynuclear assemblies with **L10**, in which the proportion of intramolecular interactions is minimised. It is shown that an a priori prediction of the effective concentration in tripodal systems must take into account both entropic and enthalpic contributions.

Experimental Section

General: Chemicals were purchased from Acros Organics, Fluka and Aldrich and used without further purification unless otherwise stated. Acetonitrile was distilled over CaH_2. **L10** and its lanthanide complexes with selected Ln^{III} ions were synthesised according to the published procedures.[22]

Data for isolated compounds

$[Nd_4\mathbf{L10}_4][ClO_4]_{12}$: ^{1}H NMR ($CD_3CN$): $\delta = -8.05$ (s, 1H, CH_3), -0.55 (s, 3H, CH_3), 1.65 (s, 3H, CH_3), 1.99 (m, 1H, CH_2), 2.42 (m, 1H, CH_2), 2.50 (m, 1H, CH_2), 3.06 (m, 1H, CH_2), 4.25–4.29 (m, 2H, CH_2), 10.05 (s, 1H, CH), 10.22 (s, 1H, CH), 10.49 (s, 1H, CH), 11.3 ppm (s, 1H, NH); ESMS (CH_3CN): *m/z* calcd for $\{[Nd_4\mathbf{L10}_4][ClO_4]_8\}^{4+}$: 1073.1; found: 1073.2; elemental analysis calcd (%) for $[Nd_4(C_{38}H_{51}N_9O_6)_4][ClO_4]_{12}\cdot 10.5H_2O$: C 37.40, H 10.33, N 4.65; found: C 37.41, H 10.29, N 4.55.

$[Yb_4\mathbf{L10}_4][ClO_4]_{12}$: ^{1}H NMR ($CD_3CN$): $\delta = 1.11$ (s, 1H, CH_3), 2.51 (m, 1H, CH_2), 2.62 (m, 1H, CH_2), 3.65 (s, 1H, CH), 4.09 (m, 1H, CH_2), 4.33 (s, 1H, CH), 4.44 (s, 1H, CH), 6.12 (m, 1H, CH_2), 6.55 (s, 3H, CH_3), 6.61 (s, 1H, NH), 8.26 (m, 1H, CH_2), 9.47 (m, 1H, CH_2), 31.07 ppm (s, 1H, CH_3); elemental analysis calcd (%) for $[Yb_4(C_{38}H_{51}N_9O_6)_4][ClO_4]_{12}\cdot 13.4H_2O$: C 36.18, H 9.99, N 4.61; found: C 36.18, H 9.92, N 4.50.

$[Y_4\mathbf{L10}_4][ClO_4]_{12}$: ^{1}H NMR ($CD_3CN$): $\delta = 0.41$ (s, 1H, CH_3), 0.76 (t, $J = 7$ Hz, 3H, CH_3), 1.47 (t, $J = 7$ Hz, 3H, CH_3), 2.86 (m, 1H, CH_2), 3.07 (m, 1H, CH_2), 3.23 (m, 1H, CH_2), 3.24 (m, 1H, CH_2), 3.77 (m, 1H, CH_2), 3.95 (m, 1H, CH_2), 8.08 (d, $J = 8$ Hz, 1H, CH), 8.33 (d, $J = 8$ Hz, 1H, CH), 8.34 (t, 1H, NH), 8.68 ppm (t, $J = 8$ Hz, 1H, CH); ESMS (CH_3CN): *m/z* calcd for $\{[Y_4\mathbf{L10}_4][ClO_4]_8\}^{4+}$: 1017.8; found: 1017.7; elemental analysis calcd (%) for $[Y_4(C_{38}H_{51}N_9O_6)_4][ClO_4]_{12}\cdot 11H_2O$: C 39.11, H 10.78, N 4.79; found: C 39.11, H 10.74, N 4.82.

*[Lu$_3$**L10**$_2$][ClO$_4$]$_9$*: ^{1}H NMR (CD_3CN): see Table S8; ESMS (CH_3CN): *m/z* calcd for $\{[Lu_3(\mathbf{L10})]_2[ClO_4]_6\}^{3+}$: 860.6; found: 860.8; elemental analysis calcd (%) for $[Lu_3(C_{38}H_{51}N_9O_6)_2][ClO_4]_9 \cdot 5.8H_2O$: C 30.59, H 8.45, N 3.84; found: C 30.72, H 8.15, N 4.08.

Spectroscopic and analytical measurements: UV/Vis electronic spectra of the complexes were recorded in solution in CH_3CN by using a Perkin–Elmer Lambda 900 spectrometer with quartz cells of 0.1 cm path length. Mathematical treatment of the spectrophotometric titrations was performed with the SPECFIT program.[39] ^{1}H and ^{13}C spectra were recorded by using a high-field NMR spectrometer (400 MHz, Bruker). Chemical shifts are given in ppm. Standard electrospray mass spectra (ESMS) were recorded by using an API 150EX LC/MS system (Applied Biosystems/MDS SCIEX). ESMS spectra of Ln^{III} complexes were recorded in 10^{-4} M acetonitrile solutions by using a Finnigan SSQ7000 instrument at the optimised ionisation temperature (150 °C). Excitation and emission spectra and lifetime measurements were recorded by using a Perkin–Elmer LS-50B spectrometer equipped for low-temperature measurements. Lifetimes were averaged over three independent determinations. High-resolution emission and excitation spectra of solid samples were measured by using a Horiba Fluorolog 3 instrument. The system used for detection consisted of a Spex 270M monochromator, a Hamamatsu photomultiplier and a Tektronix TDS 540B oscilloscope. Luminescence spectra and decay in solution were recorded by using a Perkin–Elmer LS-50 spectrometer. The quantum yield of $[Eu_4\mathbf{L10}_4][ClO_4]_{12}$ in acetonitrile was calculated according to the equation $\Phi_x/\Phi_r = (A_r(\bar{\nu})I_r(\bar{\nu})n_x^2D_x)/(A_x(\bar{\nu})I_x(\bar{\nu})n_r^2D_r)$, in which *x* refers to the sample and *r* to the reference (the solution of $[Eu(terpy)_3][ClO_4]_3$ in acetonitrile[29]), *A* is the absorbance, $\bar{\nu}$ is the excitation wavenumber, *I* is the intensity of the excitation light at this energy, *n* is the refractive index and *D* is the integrated emitted intensity. The calculation of the Conolly surfaces was performed by using the Jmol program[44] by considering acetonitrile molecule as a probe ($r = 2.0$ Å). The distribution curves were computed by using the HySS2 program.[45] Optimisation of the molecular model of the hypothetical mononuclear complex with **L10** was performed by using the Gaussian 03 program[46] with the symmetry constraint (C_3) at the DFT level (Perdew–Wang 91)[47] by using DZVP (double-ζ basis set + polarisation),[48] except for Eu (pseudopotential of Dolg et al.).[49] Elemental analyses were performed by Dr. H. Eder and K.-L. Buchwalder from the University of Geneva and the results are summarised in Table S1.

Acknowledgements

We thank Philippe Perottet for recording the ESMS spectra. We acknowledge Prof. A. Hauser for providing access to spectroscopy equipment. Financial support from the University of Geneva and SNF are gratefully acknowledged.

[1] a) G. R. Choppin in *Lanthanide Probes in Life, Chemical and Earth Sciences*, Elsevier, Amsterdam, **1989**, Chapter 1; b) J.-C. G. Bünzli in *Rare Earths* (Eds.: R. Saez Puche, P. Caro), Editorial Complutense, Madrid, **1998**, pp. 223–259; c) J.-C. G. Bünzli, *Spectroscopic Properties of Rare Earth in Optical Materials, Vol. 83* (Eds.: G. K. Liu, B. Jacquier), Springer, Berlin, **2005**, Chapter 11; d) J.-C. G. Bünzli, C. Piguet, *Chem. Soc. Rev.* **2005**, *34*, 1048–1077.

[2] a) T. Jüstel, H. Nikol, C. Ronda, *Angew. Chem.* **1998**, *110*, 3250–3271; *Angew. Chem. Int. Ed.* **1998**, *37*, 3084–3103; b) S. Capecchi, O. Renault, G. Moon, M. Halim, M. Etchells, P. J. Dobson, O. V. Salata, V. Christou, *Adv. Mater.* **2000**, *12*, 1591–1594; c) F. Liang, Q. Zhou, Y. Cheng, L.-Y. Wang, D. Ma, X. Jing, F. Wang, *Chem. Mater.* **2003**, *15*, 1935–1937.

[3] a) J.-C. G. Bünzli, P. Froidevaux, C. Piguet, *Adv. Mater. Res.* **1994**, *1–2*, 1–10; b) C. Edder, C. Piguet, J.-C. G. Bünzli, G. Hopfgartner, *J. Chem. Soc. Dalton Trans.* **1997**, 4657–4663.

[4] J. Kido, Y. Okamoto, *Chem. Rev.* **2002**, *102*, 2357–2368.

[5] a) I. Hemmilä, T. Ståhlberg, P. Mottram, *Bioanalytical Applications of Labelling Technologies*, Wallac Oy, Turku, **1995**; b) G. Mathis in *Rare Earths* (Eds: R. Saez Puche and P. Caro.), Editorial Complutense, Madrid, **1998**, pp. 285–298; c) K. Matsumoto, J. G. Yuan in *Metal Ions in Biological Systems, Vol. 40* (Eds.: A. Sigel, H. Sigel), Marcel Dekker, New York, **2003**, Chapter 6.

[6] a) T. Gunnlaugsson, J. P. Leonard, *Dalton Trans.* **2005**, 3204–3212; and references therein; b) J. P. Leonard, T. Gunnlaugsson, *J. Fluoresc.* **2005**, *15*, 585–595.

[7] a) K. Kuriki, Y. Koike, Y. Okamoto, *Chem. Rev.* **2002**, *102*, 2347–2356; b) J. W. Stouwdam, G. A. Hebbink, J. Huskens, F. C. J. M. Van Veggel, *Chem. Mater.* **2003**, *15*, 4604–4616.

[8] a) P. Caravan, J. J. Ellison, T. J. McMurry, R. B. Lauffer, *Chem. Rev.* **1999**, *99*, 2293–2352; b) *The Chemistry of Contrast Agents in Medical Magnetic Resonance Imaging* (Eds.: A. E. Merbach, E. Toth), Wiley, New York, **2001**.

[9] For examples of tetraazamacrocyclic derivatives, see: a) P. Hermann, J. Kotek, V. Kubicek, I. Lukes, *Dalton Trans.* **2008**, 3027–3047; b) C. P. Montgomery, B. S. Murray, E. J. New, R. Pal, D. Parker, *Acc. Chem. Res.* **2009**, *42*, 925–937; for examples of triazamacrocyclic ligands, see: c) L. Tei, G. Baum, A. J. Blake, D. Fenske, M. Schröder, *J. Chem. Soc. Dalton Trans.* **2000**, 2793–2799; d) L. J. Charbonnière, R. Ziessel, M. Guardigli, A. Roda, N. Sabbatini, M. Cesario, *J. Am. Chem. Soc.* **2001**, *123*, 2436–2437; e) A. Nonat, C. Gateau, P. H. Fries, M. Mazzanti, *Chem. Eur. J.* **2006**, *12*, 7133–7150.

[10] a) D. Imbert, S. Comby, A.-S. Chauvin, J.-C. G. Bünzli, *Chem. Commun.* **2005**, 1432–1434; b) S. Comby, D. Imbert, A.-S. Chauvin, J.-C. G. Bünzli, *Inorg. Chem.* **2006**, *45*, 732–743; c) N. Chatterton, Y. Bretonniere, J. Pecaut, M. Mazzanti, *Angew. Chem.* **2005**, *117*, 7767–7770; *Angew. Chem. Int. Ed.* **2005**, *44*, 7595–7598.

[11] a) F. Renaud, C. Piguet, G. Bernardinelli, J.-C. G. Bünzli, G. Hopfgartner, *J. Am. Chem. Soc.* **1999**, *121*, 9326–9342; b) F. Renaud, C. Decurnex, C. Piguet, G. Hopfgartner, *J. Chem. Soc. Dalton Trans.* **2001**, 1863–1871.

[12] J.-M. Senegas, G. Bernardinelli, D. Imbert, J.-C. G. Bünzli, P.-Y. Morgantini, J. Weber, C. Piguet, *Inorg. Chem.* **2003**, *42*, 4680–4695.

[13] Y. Bretonnière, R. Wietzke, C. Lebrun, M. Mazzanti, J. Pécaut, *Inorg. Chem.* **2000**, *39*, 3499–3505.

[14] Y. Bretonnière, M. Mazzanti, R. Wietzke, J. Pécaut, *Chem. Commun.* **2000**, 1543–1544.

[15] a) G. Tallec, D. Imbert, P. H. Fries, M. Mazzanti, *Dalton Trans.* **2010**, *39*, 9490–9492; b) S. Comby, D. Imbert, C. Vandevyver, J.-C. G. Bunzli, *Chem. Eur. J.* **2007**, *13*, 936–944.

[16] a) C. J. Jocher, E. G. Moore, J. Xu, S. Avedano, M. Botta, S. Aime, K. N. Raymond, *Inorg. Chem.* **2007**, *46*, 9182–9191; b) M. Seitz, M. D. Pluth, K. N. Raymond, *Inorg. Chem.* **2007**, *46*, 351–353; c) E. G. Moore, J. Xu, C. J. Jocher, I. Castro-Rodriguez, K. N. Raymond, *Inorg. Chem.* **2008**, *47*, 3105–3118.

[17] a) S. Koeller, G. Bernardinelli, C. Piguet, *Dalton Trans.* **2003**, 2395–2404; b) S. Koeller, G. Bernardinelli, B. Bocquet, C. Piguet, *Chem. Eur. J.* **2003**, *9*, 1062–1074.

[18] G. Canard, S. Koeller, G. Bernardinelli, C. Piguet, *J. Am. Chem. Soc.* **2008**, *130*, 1025–1040.

[19] a) J. Hamacek, M. Borkovec, C. Piguet, *Chem. Eur. J.* **2005**, *11*, 5217–5226; b) J. Hamacek, M. Borkovec, C. Piguet, *Chem. Eur. J.* **2005**, *11*, 5227–5237; c) G. Ercolani, C. Piguet, M. Borkovec, J. Hamacek, *J. Phys. Chem. B* **2007**, *111*, 12195–12203.

[20] G. Canard, C. Piguet, *Inorg. Chem.* **2007**, *46*, 3511–3522.

[21] B. El Aroussi, N. Dupont, G. Bernardinelli, J. Hamacek, *Inorg. Chem.* **2010**, *49*, 606–615.

[22] J. Hamacek, G. Bernardinelli, Y. Filinchuk, *Eur. J. Inorg. Chem.* **2008**, 3419–3422.

[23] a) O. Mamula, M. Lama, H. Stoeckli-Evans, S. Shova, *Angew. Chem.* **2006**, *118*, 5062–5066; *Angew. Chem. Int. Ed.* **2006**, *45*, 4940–4944; b) C. He, Z. Lin, Z. He, C. Duan, C. Xu, Z. Wang, C. Yan, *Angew. Chem.* **2008**, *120*, 891–895; *Angew. Chem. Int. Ed.* **2008**, *47*, 877–881; c) J. Xu, K. N. Raymond, *Angew. Chem.* **2000**, *112*, 2857–2859; *Angew. Chem. Int. Ed.* **2000**, *39*, 2745–2747; d) Y. Bretonnière, M. Mazzanti, J. Pécaut and M. M. Olmstead, *J. Am. Chem. Soc.*

2002, *124*, 9012–9013; e) T. Kajiwara, H. Wu, T. Ito, N. Iki and S. Miyano, *Angew. Chem.* **2004**, *116*, 1868–1871; *Angew. Chem. Int. Ed.* **2004**, *43*, 1832–1835.

[24] a) S. Zebret, N. Dupont, G. Bernardinelli, J. Hamacek, *Chem. Eur. J.* **2009**, *15*, 3355–3358; b) G. Bozoklu, C. Marchal, C. Gateau, J. Pécaut, D. Imbert, M. Mazzanti, *Chem. Eur. J.* **2010**, *16*, 6159–6163; c) R. Hedinger, M. Ghisletta, K. Hegetschweiler, E. Toth, A. E. Merbach, R. Sessoli, D. Gatteschi, V. Gramlich, *Inorg. Chem.* **1998**, *37*, 6698–6705; d) J.-M. Senegas, S. Koeller, C. Piguet, *Chem. Commun.* **2005**, 2235–2237.

[25] C. Piguet, G. Bernardinelli, G. Hopfgartner, *Chem. Rev.* **1997**, *97*, 2005–2062.

[26] S. Rigault, C. Piguet, G. Bernardinelli, G. Hopfgartner, *Angew. Chem.* **1998**, *110*, 178–181; *Angew. Chem. Int. Ed.* **1998**, *37*, 169–172.

[27] F. Renaud, C. Piguet, G. Bernardinelli, J.-C. G. Bünzli, G. Hopfgartner, *Chem. Eur. J.* **1997**, *3*, 1660–1667.

[28] S. T. Frey, W. D. Horrocks, Jr., *Inorg. Chim. Acta* **1995**, *229*, 383–390.

[29] S. Petoud, J.-C. G. Bünzli, C. Piguet, Q. Xiang, R. Thummel, *J. Lumin.* **1999**, *82*, 69–79.

[30] a) W. D. Horrocks, Jr., D. R. Sudnick, *Acc. Chem. Res.* **1981**, *14*, 384–392; b) R. C. Holz, C. A. Chang, W. D. Horrocks, Jr., *Inorg. Chem.* **1991**, *30*, 3270–3275; c) A. Beeby, J. M. Clarkson, R. S. Dickins, S. Faulkner, D. Parker, L. Royle, A. S. d. Sousa, J. A. G. Williams, M. Woods, *J. Chem. Soc. Perkin Trans. 1* **1999**, *1*, 493–503.

[31] Crystal data for $[\{Lu_3(C_{38}H_{51}N_9O_6)_2(H_2O)_6\}_3][ClO_4]_9 \cdot [H_2O]_9$: $M_r = 3131.76$; hexagonal; space group $P6_3$; $a = 21.805(12)$, $c = 15.828(15)$ Å; $V = 6517(8)$ Å^3, $\rho = 1.596$ g cm^{-3}; $\mu = 2.54$ mm^{-1}; $Z = 2$; $\lambda = 0.71073$ Å; $T = 120$ K; 49723 reflections collected; 9218 reflections independent ($R_{int} = 0.044$) and 8635 observed reflections [$F^2 > 2\sigma(F^2)$]; 569 refined parameters; $R = 0.049$; $wR = 0.108$; Flack parameter 0.061(12). CCDC-808290 contains the supplementary crystallographic data for this paper. These data can be obtained free of charge from The Cambridge Crystallographic Data Centre via www.ccdc.cam.ac.uk/data_request/cif.

[32] a) N. Dalla Favera, L. Guenee, G. Bernardinelli, C. Piguet, *Dalton Trans.* **2009**, 7625–7638; b) T. Riis-Johannessen, G. Bernardinelli, Y. Filinchuk, S. Clifford, N. Dalla Favera, C. Piguet, *Inorg. Chem.* **2009**, *48*, 5512–5525.

[33] a) D. Zuccaccia, A. Macchioni, *Organometallics* **2005**, *24*, 3476–3486; b) A. Macchioni, G. Ciancaleoni, C. Zuccaccia, D. Zuccaccia, *Chem. Soc. Rev.* **2008**, *37*, 479–489.

[34] a) A. Spernol, K. Z. Wirtz, *Z. Naturforsch. A* **1953**, *8*, 522–532; b) A. Gierer, K. Z. Wirtz, *Z. Naturforsch. A* **1953**, *8*, 532–538.

[35] H.-C. Chen, S.-H. Chen, *J. Phys. Chem.* **1984**, *88*, 5118–5121.

[36] S. J. Candau in *Surfactant Solutions* (Ed.: R. Zana), Marcel Dekker, New York, **1987**, pp. 157–158.

[37] a) M. L. Connolly, *Science* **1983**, *221*, 709–713; b) M. L. Connolly, *J. Appl. Crystallogr.* **1983**, *16*, 548–553.

[38] a) J. Perrin, *J. Phys. Radium* **1934**, *5*, 497–511; b) J. Perrin, *J. Phys. Radium* **1936**, *7*, 1–11; c) R. F. Probstein, *Physicochemical Hydrodynamics: An Introduction*, Wiley, New York, **1994**, pp. 111–114.

[39] H. Gampp, M. Maeder, C. J. Meyer, A. D. Zuberbuehler, *Talanta* **1986**, *33*, 943–951.

[40] a) K. Zeckert, J. Hamacek, J.-M. Senegas, N. Dalla-Favera, S. Floquet, G. Bernardinelli, C. Piguet, *Angew. Chem.* **2005**, *117*, 8168–8172; *Angew. Chem. Int. Ed.* **2005**, *44*, 7954–7958; b) N. Dalla-Favera, J. Hamacek, M. Borkovec, D. Jeannerat, F. Gumy, J.-C. G. Bünzli, G. Ercolani, C. Piguet, *Chem. Eur. J.* **2008**, *14*, 2994–3005.

[41] C. Piguet, *Chem. Commun.* **2010**, *46*, 6209–6231.

[42] N. Dalla-Favera, U. Kiehne, J. Bunzen, S. Hytteballe, A. Lützen, C. Piguet, *Angew. Chem.* **2010**, *122*, 129–132; *Angew. Chem. Int. Ed.* **2010**, *49*, 125–128.

[43] **L1^a** corresponds to **L1** with $n = 1$. The average value of c^{eff} was extracted for La, Ce and Pr complexes with **L1^a** (Ref. [11a]) from the stability constants of mononuclear species $[Ln\mathbf{L1}^a]^{3+}$ and $[Ln\mathbf{L1}^a{}_2]^{3+}$ by using thermodynamic modelling (see the Supporting Information for further details).

[44] Jmol: an open source Java viewer for chemical structures in 3D, http://www.jmol.org/.

[45] L. Alderighi, P. Gans, A. Ienco, D. Peters, A. Sabatini, A. Vacca, *Coord. Chem. Rev.* **1999**, *184*, 311–318.

[46] Gaussian 03, Revision B.03, M. J. Frisch, G. W. Trucks, H. B. Schlegel, G. E. Scuseria, M. A. Robb, J. R. Cheeseman, J. A. Montgomery, Jr., T. Vreven, K. N. Kudin, J. C. Burant, J. M. Millam, S. S. Iyengar, J. Tomasi, V. Barone, B. Mennucci, M. Cossi, G. Scalmani, N. Rega, G. A. Petersson, H. Nakatsuji, M. Hada, M. Ehara, K. Toyota, R. Fukuda, J. Hasegawa, M. Ishida, T. Nakajima, Y. Honda, O. Kitao, H. Nakai, M. Klene, X. Li, J. E. Knox, H. P. Hratchian, J. B. Cross, V. Bakken, C. Adamo, J. Jaramillo, R. Gomperts, R. E. Stratmann, O. Yazyev, A. J. Austin, R. Cammi, C. Pomelli, J. W. Ochterski, P. Y. Ayala, K. Morokuma, G. A. Voth, P. Salvador, J. J. Dannenberg, V. G. Zakrzewski, S. Dapprich, A. D. Daniels, M. C. Strain, O. Farkas, D. K. Malick, A. D. Rabuck, K. Raghavachari, J. B. Foresman, J. V. Ortiz, Q. Cui, A. G. Baboul, S. Clifford, J. Cioslowski, B. B. Stefanov, G. Liu, A. Liashenko, P. Piskorz, I. Komaromi, R. L. Martin, D. J. Fox, T. Keith, M. A. Al-Laham, C. Y. Peng, A. Nanayakkara, M. Challacombe, P. M. W. Gill, B. Johnson, W. Chen, M. W. Wong, C. Gonzalez, J. A. Pople, Gaussian, Inc., Wallingford CT, **2004**.

[47] J. P. Perdew, Y. Wang, *Phys. Rev. B* **1996**, *54*, 16533–16539.

[48] N. Godbout, D. R. Salahub, J. Andzelm, E. Wimmer, *Can. J. Chem.* **1992**, *70*, 560–571.

[49] a) M. Dolg, H. Stoll, A. Savin, H. Preuss, *Theor. Chim. Acta* **1989**, *75*, 173–194; b) M. Dolg, H. Stoll, A. Savin, H. Preuss, *Theor. Chim. Acta* **1993**, *85*, 441–450.

Received: January 17, 2011
Published online: May 5, 2011

